Eur. Phys. J. C (2022) 82:1087
https://doi.org/10.1140/epjc/s10052-022-11045-x

THE EUROPEAN PHYSICAL JOURNAL C

Regular Article - Theoretical Physics

D-dimensional dyonic AdS black holes with quasi-topological electromagnetism in Einstein Gauss–Bonnet gravity

Yassine Sekhmani[1,a], **Hicham Lekbich**[2,3], **Abderrahman El Boukili**[3], **Moulay Brahim Sedra**[2]

[1] Département de Physique, Equipe des Sciences de la matière et du rayonnement, ESMaR, Faculté des Sciences, Université Mohammed V de Rabat, Rabat, Morocco
[2] Département de Physique, Laboratoire de physique des Matériaux et Subatomique, LPMS, Faculté des Sciences, Université Ibn Tofail, Kenitra, Morocco
[3] Department of Physics, Faculty of Science and Technics, University of Moulay Ismail, BP 509, Boutalamine, 52000 Errachidia, Morocco

Received: 10 May 2022 / Accepted: 16 November 2022 / Published online: 2 December 2022

Abstract Within Gauss–Bonnet gravity, we construct a solution endowed with dyonic matter fields in a higher dimension. The quasi-topological electromagnetism generates two kinds of contributions; one is the kinetic terms, and the second refers to the interactif terms. This overcomes the invariance topological problem. We investigate the thermodynamical proprieties of the obtained solution, namely, ADM mass, Hawking temperature, and entropy. To inspect the local stability, we examine the associated heat capacity. With regards to optical proprieties, we analyze the null geodesic in terms of the given parameter space. The shadow radius is a generating form with all the physical parameters that govern the shadow behavior. The study restricts only the taking of the effects of the D and α parameters. Finally, we examine the impact of the dimension D, GB coupling constant α, the cosmological constant Λ, the electric q_e, the magnetic charge q_m and the coupling constant β on the energy emission rate.

1 Introduction

Quasi-topological electromagnetism [1] is considered as an alternative way restoring the dynamic contribution at the level of the equation of motion. The fact that the Maxwell field strength is a topological invariant, as well as the Riemann curvature tensor, all of which are 2-forms.

$$\int tr(R \wedge R), \quad \int F \wedge F. \tag{1.1}$$

These quantities remain independent of the spacetime metric. To obtain dependancy with the metric, it is necessary to take into consideration another purely magnetic field yielding dyonic objects. The starting point is the introduction of supplemented terms within the corresponding lagrangian, which are related to topological invariants.Indeed, in dimension $D = 2k$, any $2k$-forms Maxwell field strength is used to build the topological structure, $V_{[2k]} = F_{[2]} \wedge F_{[2]} \wedge \cdots \wedge F_{[2]}$. In order to carry out this treatment, we consider the squared norm combining both electric and magnetic field strengths as follows

$$U^{(k)}_{[D]} \sim |V_{[2k]}|^2 \sim V_{[2k]} \wedge \star V_{[2k]}. \tag{1.2}$$

The particular case $k = 1$ refers to the Maxwell term. Consequently, these invariants remove the noncontribution to the field equations.

In recent years, the thermodynamics of black holes has attracted a lot of interest in the field of theoretical physics. Since then, several studies have been conducted in favor of constructing a thermodynamic framework using the techniques of classical physics [2–5]. Kastor, Ray, and Traschen [6] were the first to invent the extended version of phase space thermodynamics, also known as black hole chemistry [7], to focus on this goal. The fundamental idea of this approach requires the consideration that pressure is a negative cosmological constant. Mass has the property of being the enthalpy in this formulation. The equation of state $P - v$ accurately represents the small-large black hole phase transition in AdS black holes from the point of view of the liquid-gas in the Van der Waals (VdW) fluid [8]. To consider AdS black holes as heat engines [9,10], the variables P and V are used. On the other hand, many contributions have affected the development of gravity models, leading to a new understanding of thermodynamics. By the way, the AdS/CFT duality [11], also known as the holographic principle [12,13], allows a better understanding of the nature of microscopic degrees of freedom, which contributes to the entropy of the black hole.

[a] e-mail: sekhmaniyassine@gmail.com (corresponding author)

According to this duality, the dual field theory thermal state is identical to the location of the AdS black hole state in the mass.

Lanczos D. Lovelock [14–16] discovered a natural extension framework for Einstein's theory to higher dimensions. In a special dimension, the Lovelock lagrangian gets different theoretical aspects. More specifically, in three and four dimensions ($D = 3, 4$), Lovelock's theory reduces to Einstein's theory. The second order of the Lovelock theory corresponds to the quadratic tensor of the Gauss–Bonnet term, which turns into a topological surface term and starts being non-trivial in $D = 5$ dimensions. On the other hand, there was the most linked investigation concerning the Lovelock gravities in the context of cosmological models [17] and in the cosmological background through string theories. Furthermore, the quadratic Gauss–Bonnet term appropriate to the 2nd order of Lovelock gravities in four dimensions can be derived from the low energy effective action of heterotic string theory [18–21] and also formed in the six-dimensional *Calabi–Yau* compactification of M-theory [22,23], and the theory is free of ghosts of other exactions [24,25]. After all, a few insights into the quadratic term of Gauss–Bonnet were elaborated in the frame of a spherical black hole by Boulware and Deser in $D > 5$ spacetime [24–27]. Recent works on Gauss–Bonnet theory have succeeded in interpreting the $4D$ topological invariant by rescaling the GB coupling constant [28]. As a result, the EGB theory becomes a fruitful sector to explore black hole properties [29–31].

The observation of a black hole shadow offers a technique to deal with topological background, in a way that both shape and size are given in terms of the black hole parameters. Generally, the shadow of a Schwarzschild–Tangherlini black hole is perfectly circular [32], but for a Kerr black hole, the shadow is distorted [33]. Recent observations have managed to show, with the help of informatics data, a simulated image with regard to black objects. Roughly speaking, the M87* picture [34,35], yielded an intensive study of the black hole shadow in different gravity models [36–43].

The outline of this paper is as follows: in Sect. 2, we built a D-dimensional black solution in the frame of EGB gravity with a quasitopological electromagnetism source. Section 3 is devoted to computing the relevant thermodynamic quantities and analyzing the local stability. In Sect. 4, we investigate the optical proprieties of our black hole solution.

2 Einstein Gauss–Bonnet with quasitopological electromagnetism

2.1 The set up

The attempt to have a non-linear electrodynamic field as a source of matter in the context of such a gravity model is governed by the Born–Infeld term [44] as the main and first model. The pursuit of this model opens the way for new models such as Euler–Heisenberg [45], ModMax [46], etc. As inspired by these models, quasitopological electromagnetism is considered to be another non-linear electrodynamic field. Certainly, this model borrows ideas from the topological gravity model [47–50].

An overview of dyonic fields is dedicated to experiencing the situation of a purely electric source [1] with a part of the magnetic field together in a quasi-topological electromagnetism [51,52]. However, a convenient choice for the gauges fields should be in the following form

$$F_{\mu\nu} \sim h'(r)\delta^{x^0 x^1}_{\mu\nu}, \quad H_{\rho_1\cdots\rho_p} \sim \delta^{x^2\cdots x^D}_{\rho_1\cdots\rho_p}, \tag{2.1}$$

with $p = D - 2$, in which $F_{\mu\nu}$ and $H_{\rho_1\cdots\rho_p}$ are the electric and magnetic field strength, respectively. From the gauge field structure, it is worth noting that the only non-vanishing terms are the gauges Kinetic $|\mathcal{F}_{[2]}|^2 \sim F_{\mu\nu}F^{\mu\nu}$ and $|\mathcal{H}_{[p]}|^2$, and an interaction term $|\mathcal{F}\mathcal{H}_{[D]}|^2$ mentioned above. Indeed, one can consider the following quantities:

$$\mathcal{F}_{[2k]} = F_{[2]} \wedge F_{[2]} \wedge \cdots \wedge F_{[2]}, \quad k \leq \lfloor D/2 \rfloor, \tag{2.2}$$

$$\mathcal{H}_{[pk]} = H_{[p]} \wedge H_{[p]} \wedge \cdots \wedge H_{[p]} \quad k \leq \lfloor D/p \rfloor, \tag{2.3}$$

$$\mathcal{F}\mathcal{H}_{[2k+pl]} = \mathcal{F}_{[2k]} \wedge \mathcal{H}_{[pl]}, \quad \{2k + p\ell \leq D\}. \tag{2.4}$$

The present step is devoted to constructing the corresponding physical Lagrangian, where the squared norms $|\mathcal{F}_{[2k]}|^2$, $|\mathcal{H}_{[pk]}|^2$ and $|\mathcal{F}\mathcal{H}_{[2k+p\ell]}|^2$ are given in a component notation after using the Hodge product

$$|\mathcal{F}_{[2k]}|^2 \sim \delta^{\rho_1\cdots\rho_{2k}}_{\sigma_1\cdots\sigma_{2k}} F_{\rho_1\rho_2}F_{\rho_3\rho_4}\cdots F_{\rho_{2k-1}\rho_{2k}}F^{\sigma_1\sigma_2}F^{\sigma_3\sigma_4}\cdots F^{\sigma_{2k-1}\sigma_{2k}}, \tag{2.5}$$

$$|\mathcal{H}_{[pk]}|^2 \sim \delta^{\rho_1\cdots\rho_{pk}}_{\sigma_1\cdots\sigma_{pk}} H_{\rho_1\cdots\rho_p}\cdots H_{\cdots\rho_{pk}}H^{\sigma_1\cdots\sigma_p}\cdots H^{\cdots\sigma_{pk}}, \tag{2.6}$$

$$|\mathcal{F}\mathcal{H}_{2k+p\ell}|^2 \sim \delta^{\rho_1\cdots\rho_{2k+p\ell}}_{\sigma_1\cdots\sigma_{2k+p\ell}} F_{\rho_1\rho_2}H_{\rho_3\cdots\rho_{p+2}}\cdots F_{\ldots}H_{\cdots\rho_{2k+p\ell}}F^{\sigma_1\sigma_2}H^{\sigma_3\cdots\sigma_{p+2}}\cdots F\cdots H^{\cdots\sigma_{2k+p\ell}}, \tag{2.7}$$

where $\delta^{\rho_1\cdots\rho_{2k}}_{\sigma_1\cdots\sigma_{2k}}$ denotes the rank-$4k$ skew-symmetric Kronecker delta. While other quadratic terms can arise differently in a mixed manner between the above quantities, as $\mathcal{F}_{[2k]} \wedge *\mathcal{H}_{[p\ell]}$ with $2k = p\ell$ and $k \leq \lfloor D/2 \rfloor$, $\mathcal{F}_{[2k]} \wedge *\mathcal{F}\mathcal{H}_{[2q+p\ell]}$ with $p\ell = 2(k-q)$ and $k \leq \lfloor D/2 \rfloor$ where $\lfloor\,\rfloor$ is the floor function, as well as $\mathcal{H}_{[pk]} \wedge *\mathcal{F}\mathcal{H}_{[2q+p\ell]}$ with $2q = p(k-\ell)$ and $k \leq \lfloor D/p \rfloor$. Basically, all these invariant quantities contribute reasonably to the field equations and, therefore, formulate the matter part of the considered action.

Consequently, we consider a D-dimensional action referred to a gravity sector in the essence of the Einstein Gauss–Bonnet theory, and in a part to a matter field labeled by a Quasi-Topological Electromagnetism in the form

$$S_D\left[g_{\mu\nu}, A_\mu, B_{\lambda_1\cdots\lambda_{p-1}}\right] = \frac{1}{16\pi}\int d^D x\sqrt{-g}\left(R - 2\Lambda + \alpha\mathcal{G} + \mathcal{L}_{QTE}\right), \quad (2.8)$$

where the matter field is represented by the following Quasi-Topological Electromagnetism Lagrangian

$$\mathcal{L}_{QTE} = -\left(\frac{1}{4}F^2 + \frac{1}{2p!}H^2 + \beta\mathcal{L}_{int}\right) \quad (2.9)$$

with $F^2 = F_{\mu\nu}F^{\mu\nu}$ and $H^2 = H_{\rho_1\cdots\rho_p}H^{\rho_1\cdots\rho_p}$, and the interaction term is given by

$$\mathcal{L}_{int} = \delta^{\lambda_1\cdots\lambda_D}_{\gamma_1\cdots\gamma_D}F_{\lambda_1\lambda_2}H_{\lambda_3\cdots\lambda_D}F^{\gamma_1\gamma_2}H^{\gamma_3\cdots\gamma_D}. \quad (2.10)$$

Here the coupling constant β has mass dimension -2.

According to Lovelock's theory of gravity, the computation must be restricted up to second order for the purpose to obtain the Einstein Gauss–Bonnet gravity. The case in which Einstein-Hilbert action arises naturally in a part of the action, in addition to the quadratic Gauss–Bonnet term given as

$$\mathcal{G} = R^2 - 4R^{\mu\nu}R_{\mu\nu} + R^{\mu\nu\rho\sigma}R_{\mu\nu\rho\sigma}. \quad (2.11)$$

The variation of the considered action given by leads to the following equation of motions

$$G_{\mu\nu} + g_{\mu\nu}\Lambda + \alpha L_{\mu\nu} = -\frac{1}{2}F_{\mu\rho}F^{\rho}_{\nu} + \frac{1}{8}g_{\mu\nu}F^2 - \frac{1}{4}\mathcal{B}_{\mu\nu} - \frac{\beta}{2}g_{\mu\nu}\mathcal{L}_{int} \quad (2.12)$$

$$\Delta_\nu F^{\nu\mu} - 4\beta\,\delta^{\mu\nu\,\gamma_1\cdots\gamma_p}_{\lambda\cdots\lambda_D}H_{\gamma_1\cdots\gamma_p}\Delta_\nu\left(F^{\lambda_1\lambda_2}H^{\gamma_3\cdots\gamma_D}\right) = 0 \quad (2.13)$$

$$\Delta H^{\mu\lambda_1\cdots\lambda_{p-1}} + 2\alpha\, p!\,\delta^{\mu\nu\rho\,\lambda_1\cdots\lambda_{p-1}}_{\gamma\cdots\gamma_D}F_{\mu\nu}\Delta_\rho\left(F^{\gamma_1\gamma_2}H^{\gamma\cdots\gamma_D}\right) = 0, \quad (2.14)$$

where $G_{\mu\nu}$ and $L_{\mu\nu}$, respectively, are the Einstein tensor and the Lanczos tensor. They are given by

$$G_{\mu\nu} = R_{\mu\nu} - \frac{1}{2}g_{\mu\nu}R, \quad (2.15)$$

$$L_{\mu\nu} = 2\left(RR_{\mu\nu} - 2R_{\mu\rho}R^{\rho}_{\nu} - 2R^{\rho\lambda}R_{\mu\nu\rho\lambda} + R^{\rho\lambda\sigma}_{\mu}R_{\nu\rho\lambda\sigma}\right) - \frac{1}{2}g_{\mu\nu}\mathcal{G}. \quad (2.16)$$

Moreover, $\mathcal{B}_{\mu\nu}$ is the energy–momentum tensor for the $B_{[p-1]}$ field. it reads

$$\mathcal{B}_{\mu\nu} = \frac{1}{(p-1)!}H_{\mu\rho_1\cdots\rho_{p-1}}H^{\rho_1\cdots\rho_{p-1}} - \frac{1}{(p!)^2}\delta^{\rho_1\cdots\rho_p\lambda}_{\sigma_1\cdots\sigma_p}(_\mu g_\nu)_\lambda H_{\rho_1\cdots\rho_p}H^{\sigma\cdots\sigma_p}. \quad (2.17)$$

An examination is carried out to determine what exactly can result from the variation of the interaction part of the Lagrangian with respect to the metric space-time. Let us now assume the following

$$\frac{1}{\sqrt{-g}}\frac{\delta\left(\sqrt{-g}\mathcal{L}_{int}\right)}{\delta g^{\mu\nu}} = X_{\mu\nu} - \frac{1}{2}g_{\mu\nu}\mathcal{L}_{int}. \quad (2.18)$$

Nevertheless these Lagrangians fulfill the identity

$$\delta^{\rho_1\cdots\rho_D}_{\sigma_1\cdots\sigma_D}F_{[\rho_1\rho_2}H_{\rho_3\cdots\rho_D}F^{\sigma_1\sigma_2}H^{\sigma_3\cdots\sigma_D}g_{\mu]\nu} = -X_{\mu\nu} + g_{\mu\nu}\mathcal{L}_{int} = 0, \quad (2.19)$$

where, this allows us to put the result

$$\frac{1}{\sqrt{-g}}\frac{\delta\left(\sqrt{-g}\mathcal{L}_{int}\right)}{\delta g^{\mu\nu}} = \frac{1}{2}g_{\mu\nu}\mathcal{L}_{int}, \quad (2.20)$$

of course, this result confirms the validity of the energy–momentum tensor with regards to the interaction Lagrangian. After that, we look for the appropriate solution pertinent to this background.

2.2 Exact solutions

In this part, we are interested in finding a physical solution to model the structure of dyonic charges within the Einstein Gauss–Bonnet theory. For that reason, we consider a static spherically symmetric metric

$$ds^2 = -f(r)dt^2 + \frac{dr^2}{f(r)} + r^2 d\Omega^2_{D-2}, \quad (2.21)$$

where one has

$$.d\Omega^2_{D-2} = d\theta_1^2 + \sum_{i=2}^{D-2}\prod_{j=1}^{i-1}\sin^2\theta_j d\theta_i^2, \quad (2.22)$$

which is the line element of $(D-2)$-dimensional unit sphere. Linking to differential geometry helps to think of a local chart $\{x^i\}$ with $i = 1, \ldots, p$, which provides an intrinsic metric ϵ_{ij} on the manifold Ω_{D-2}, with determinant ϵ. This $(D-2)$-unit sphere involves certain magnetic objects to wrap spherical $(D-2)$-cycles covered the volume form, $H_{[D-2]} \sim \mathrm{Vol}(\Omega)$, namely

$$H_{\rho_1\cdots\rho_p} = q_m\sqrt{\epsilon}\,\delta^{x^1\cdots x^p}_{\rho_1\cdots\rho_p}. \quad (2.23)$$

The Maxwell field will be purely electric,

$$F_{\mu\nu} = h'(r)\delta^{tr}_{\mu\nu} \quad (2.24)$$

where the prime denotes the derivative with respect to r. These quantities give rise to such electric and magnetic charges as

$$q_e \sim \int_{\Omega_\infty}\star F_{[2]}, \quad q_m \sim \int_{\Omega_\infty}H_{[D-2]}. \quad (2.25)$$

At this stage, making use of the Ansatz in Maxwell equations leads to find

$$r^{2p}\left[ph'(r)+rh''(r)\right]-8\beta(p!)^2q_m^2\left[ph'(r)-rh''(r)\right]=0,\quad p=D-2 \tag{2.26}$$

which admit a solution in the form

$$h'(r)=\frac{q_e r^p}{r^{2p}+8\beta(p!)^2q_m^2}. \tag{2.27}$$

A fascinating note from this solution showed that the parameter interaction and magnetic charge have similar behavior in preserving the dyonic structure of the black hole.

The next step focuses on the definition of the metric function $f(r)$. We begin to evaluate the EGB field equations (2.12), reads

$$\begin{aligned}T_t^t &= \frac{D-2}{2}\left\{\left[\frac{f'}{r}+\frac{(D-3)f}{r^2}-\frac{D-3}{r^2}\right]\right.\\ &\left.-\tilde{\alpha}\left[\frac{2ff'}{r^3}-\frac{2f'}{r^3}+\frac{(D-5)f^2}{r^4}-\frac{2(D-5)f}{r^4}+\frac{D-5}{r^4}\right]\right\},\\ T_t^t &= T_r^r,\end{aligned} \tag{2.28}$$

while the energy momentum tensor is given by

$$T_t^t=-\frac{1}{4}\left(\frac{q_m^2}{r^{2(D-2)}}+\frac{q_e^2}{r^{2(D-2)}+8\beta q_m^2\Gamma(D-1)^2}\right). \tag{2.29}$$

The fact that β is positive, results in a way that T_{tt} is a positive quantity. To simplify the computations, we consider the rescaled coupling constant

$$\tilde{\alpha}=\alpha(D-3)(D-4). \tag{2.30}$$

With these at hand, we can perform such processing to show the explicit form of $f(r)$ which is defined under a differential representation of the (t,t) part of the field equations as follows

$$\begin{aligned}&\frac{(D-3)f(r)}{r^2}-\frac{D-3}{r^2}+\frac{f'(r)}{r}\\ &+\frac{1}{4}\left(\frac{q_e^2}{8\beta q_m^2\Gamma(D-1)^2+r^{2(D-2)}}+\frac{q_m^2}{r^{2(D-2)}}\right)\\ &+\Lambda-\frac{\alpha}{2}\left(\frac{(D-5)f(r)^2}{r^4}-\frac{2(D-5)f(r)}{r^4}\right.\\ &\left.+\frac{D-5}{r^4}+\frac{2f(r)f'(r)}{r^3}-\frac{2f'(r)}{r^3}\right)=0.\end{aligned} \tag{2.31}$$

This equation provides a pair of distinct solutions referred to by the signs $\pm$. Indeed, these solutions are found to be

$$f(r)=1+\frac{r^2}{2\tilde{\alpha}}\left(1\pm\sqrt{g(r)}\right), \tag{2.32}$$

where

$$\begin{aligned}g(r)&=1+\frac{4\tilde{\alpha}m}{r^{D-1}}+\frac{8\tilde{\alpha}\Lambda}{(D-2)(D-1)}-\frac{2\tilde{\alpha}}{D-3}\\ &\times\left(q_m^2+q_e^2\,{}_2F_1\left[1,\frac{D-3}{2(D-2)};\frac{7-3D}{4-2D};\frac{-8\beta q_m^2\Gamma(D-1)^2}{r^{2D-4}}\right]\right).\end{aligned} \tag{2.33}$$

Here ${}_2F_1$ denotes Euler's hypergeometric function. In fact, the boundary conditions offer the integration constant m, which acts as a mass of the solution in a particular parameter space. Thus, the relevant ADM mass is defined according to [53] by

$$M_{ADM}=\frac{(D-2)\omega}{16\pi}m,\quad \text{with}\ \omega=\frac{2\pi^{\frac{D-1}{2}}}{\Gamma\left[\frac{D-1}{2}\right]} \tag{2.34}$$

where ω is the volume of the $(D-2)$-dimensional unit sphere.

Henceforth, the physical solution is that of the negative branch, which recovers solutions in EGB theory as well as in general relativity. It is interesting to note that every black hole solution is a given in such a parameter space, uniquely collecting all the physical parameters. Thus, our parameter space takes care of managing the set $\mathcal{M}(M,\alpha,q_e,q_m,\beta,\Lambda,D)$. Certain limits across the dynamics of the parameter space, however, are taken into account, from which the cancellation of the GB coupling constant α leads to the exploration of a solution within the framework of general relativity [51]:

$$\begin{aligned}f(r)&=1-\frac{2m}{r^{D-3}}-\frac{2\Lambda r^2}{(D-1)(D-2)}\\ &+\frac{q_m^2+q_e^2\,{}_2F_1\left[1,\frac{D-3}{2(D-2)};\frac{7-3D}{4-2D};\frac{-8\beta q_m^2\Gamma(D-1)^2}{r^{2D-4}}\right]}{2(D-2)(D-3)r^{2(D-3)}}.\end{aligned} \tag{2.35}$$

Moreover, the disappearance of the electric charge, as well as the magnetic charge, gives rise to the Tangherlini AdS-Schwarzschild solution [54]:

$$f(r)=1-\frac{2m}{r^{D-3}}-\frac{2\Lambda r^2}{(D-1)(D-2)}. \tag{2.36}$$

It is shown that Fig. 1 represents the variation of metric function against the radial coordinate. Different cases can be distinguished for the equation $f(r=r-+)=0$, among these cases, on has

- Double roots corresponding to the Cauchy horizon r_- and the event horizon r_+.
- A degenerated root $r_-=r_+=r_E$ related to an extremal black hole.
- An empty set of solutions.

Thanks to a numerical treatment, we assert unequivocally that the metric function carries at most two horizon radii for such valued parameter space. Moreover, these horizon radii can be degenerated to present one horizon radius, or no black hole system can be found. In particular, for a fixed

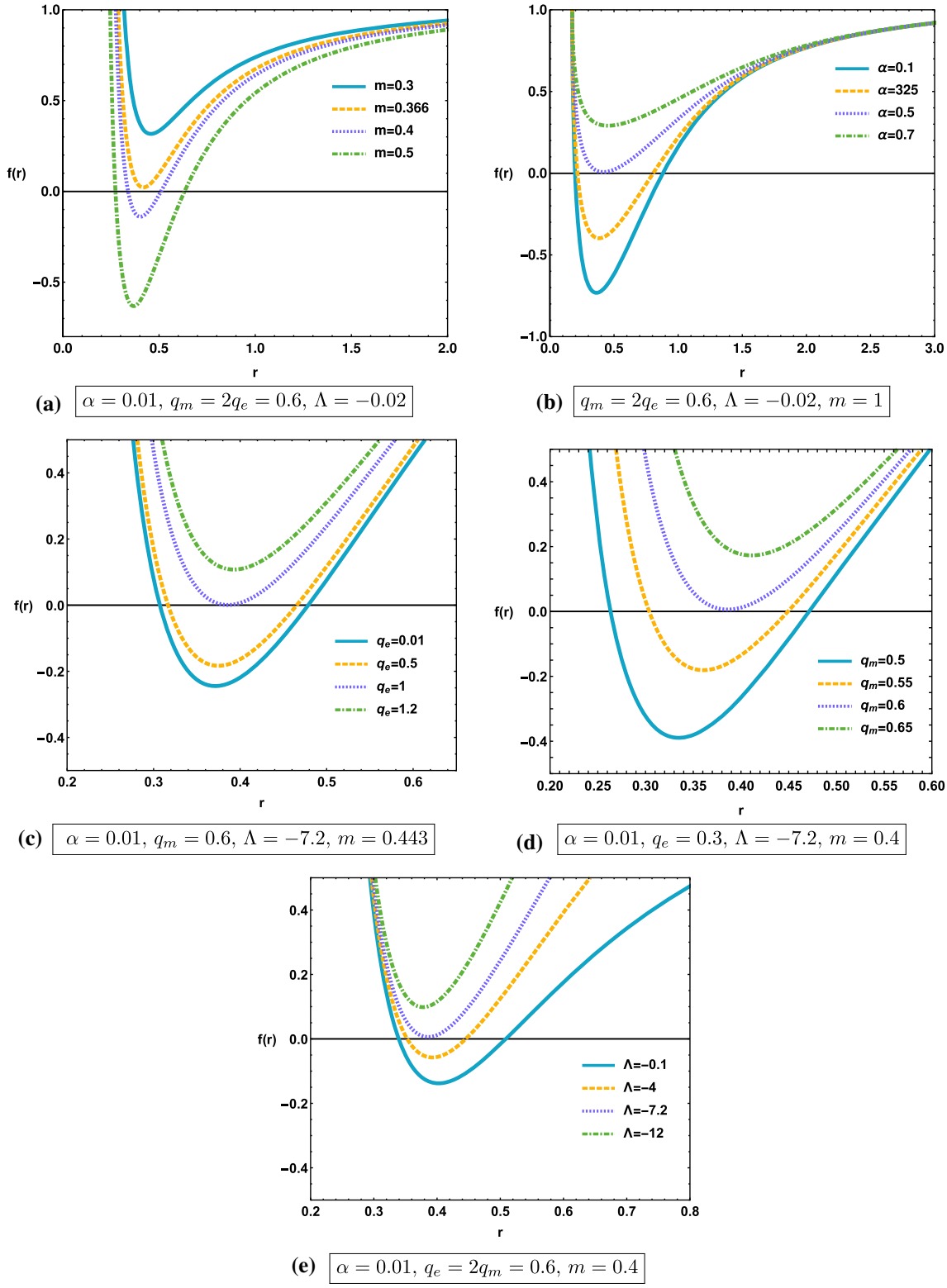

(a) $\alpha = 0.01,\ q_m = 2q_e = 0.6,\ \Lambda = -0.02$

(b) $q_m = 2q_e = 0.6,\ \Lambda = -0.02,\ m = 1$

(c) $\alpha = 0.01,\ q_m = 0.6,\ \Lambda = -7.2,\ m = 0.443$

(d) $\alpha = 0.01,\ q_e = 0.3,\ \Lambda = -7.2,\ m = 0.4$

(e) $\alpha = 0.01,\ q_e = 2q_m = 0.6,\ m = 0.4$

Fig. 1 The metric function vs radial coordinate r for several values of the parameters space with $D = 5$ and $\beta = 0.1$

value of parameters ($q_m = 2q_e = 0.6, \Lambda = -0.02, \beta = 0.1$ and $m = 1$), we find the following:

- For $D = 5, 6, 7$ if $\alpha \leq 0.3 \Rightarrow$ two horizon radius, else no horizon radius.

- For $D = 8$ if $\alpha \leq 0.4 \Rightarrow$ two horizon radius, else no horizon radius.
- For $D = 9, 10$ if $\alpha \leq 0.5 \Rightarrow$ two horizon radius, else no horizon radius.

With all this background at hand, one can explore more sides, such as thermodynamic aspects and shadow behavior.

3 Local black hole stability

In this section, we will calculate various thermodynamic quantities for our black hole. More precisely, we compute the mass of the black hole, and then we give the expression for the Hawking temperature, which allows us to calculate the related black hole entropy.

Starting with the mass of the black hole which is obtained in terms of the horizon radius r_+ by solving the equation $f(r_+) = 0$, taking into account Eq. (2.34) which gives

$$\begin{aligned} M_{ADM} = & \frac{1}{32\left(3-4D+D^2\right)\pi} r_+^{-5-D}\omega \\ & \times\Big[(D-1)\, q_m^2 r_+^8 + 2\,(D-3)\, r_+^{2D} \\ & \times\Big(\left(2-3D+D^2\right) r_+^2 \\ & + \left(24-50D+35D^2-10D^3+D^4\right)\alpha - 2r_+^4\Lambda\Big) \\ & + (D-1)\, q_e^2 r_+^8\, {}_2F_1 \\ & \times\left(1, \frac{D-3}{2\,(D-2)}, \frac{7-3D}{4-24}, -8\beta q_m^2 r_+^{4-2d}\Gamma\,[D-1]^2\right)\Big]. \end{aligned} \tag{3.1}$$

By taking $q_m = q_e = \beta = \Lambda = \alpha = 0$, Eq. (3.1) goes to the D-dimensional Schwarzschild black hole given by

$$M_{ADM} = \frac{(D-2)\omega_{D-2} r^{D-3}}{16\pi}. \tag{3.2}$$

The Hawking temperature is defined as follows

$$T_+(r_+) = \left.\frac{f'(r)}{4\pi}\right|_{r=r_+}, \tag{3.3}$$

the prime denotes the derivative with respect to r. The computations give

$$T_+ = \frac{t_1}{t_2} \tag{3.4}$$

where one has

$$\begin{aligned} t_1 = & r_+^{-2D-1}\big(8\beta q_m^2 r_+^4\Gamma(D-1)^2\big(-2r_+^{2D}\big(2\Lambda r_+^4 \\ & -(D-3)(D-2)\big(\alpha(D-5)(D-4)+r_+^2\big)\big) - q_m^2 r_+^8\big) \\ & - r_+^{2D+8}\big(q_e^2+q_m^2\big) - 2r_+^{4D}\big(2\Lambda r_+^4 \\ & -(D-3)(D-2)\big(\alpha(D-5)(D-4)+r_+^2\big)\big)\big) \end{aligned} \tag{3.5}$$

$$\begin{aligned} t_2 = & 8\pi(D-2)\left(2\alpha(D-4)(D-3)+r_+^2\right) \\ & \times\left(8\beta q_m^2 r_+^4\Gamma(D-1)^2 + r_+^{2D}\right). \end{aligned} \tag{3.6}$$

In the particular case where $q_m = q_e = \beta = \Lambda = 0$, one obtains the following well knowing form of the D-dimensional EGB Hawking temperature

$$T_+ = \frac{(D-3)\left[r_+^2+\alpha(D-5)(D-4)\right]}{4\pi r_+\left[r_+^2+2\alpha(D-4)(D-3)\right]} \tag{3.7}$$

taking $D = 5$, one obtains

$$T_+ = \frac{1}{4\pi}\left(\frac{2r_+}{r_+^2+4\alpha}\right), \tag{3.8}$$

which is the $5D$ Einstein–Gauss–Bonnet black hole temperature [55]. Furthermore, making $\alpha = 0$, one recovers the Hawking temperature of the $5D$ Schwarzschild–Tangherlini black hole given by $T_+ = (1/2\pi r)$ [56].

To investigate the behavior of the Hawking temperature, one depicts it on the Fig. 2 below:

We can see that the Hawking temperature rises to a maximum value and then drops to a minimum. It turns out that when the dimension D increases, the maximum value of the Hawking temperature also increases. Whereas this maximum is inversely proportional to the GB coupling constant.

This black hole can be regarded as a thermodynamic system only if its associated quantities obey the first-law of thermodynamics given by

$$dM = T_+ dS + \phi_e dq_e + \phi_m dq_m, \tag{3.9}$$

where the associated electric and magnetic potentials are given respectively in the following terms:

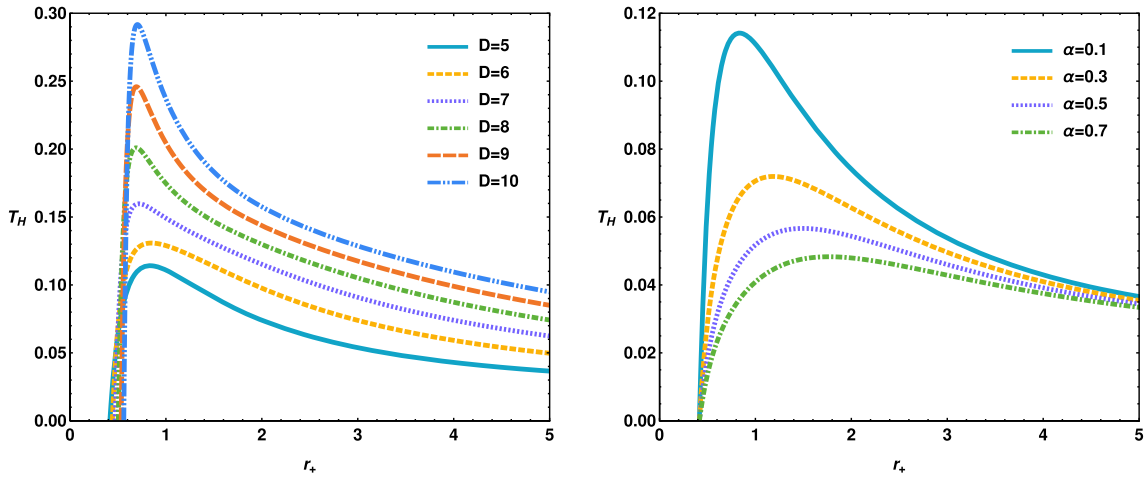

(a) $\alpha = 0.1,\ q_m = 2q_e = 0.6,\ \Lambda = -0.02,\ \beta = 0.1$ **(b)** $D = 5,\ q_m = 2q_e = 0.6,\ \Lambda = -0.02,\ \beta = 0.1$

Fig. 2 The Hawking temperature vs the event horizon for different values of D and α

$$\phi_e = \frac{\pi^{\frac{D-3}{2}} q_e r_+^{3-D}\, {}_2F_1\left(1, \frac{D-3}{2(D-2)}; \frac{7-3D}{4-2D}; -8\beta q_m^2 r_+^{4-2D}\Gamma(D-1)^2\right)}{8(D-3)\Gamma\left(\frac{D-1}{2}\right)}, \tag{3.10}$$

$$\phi_m = \frac{(D-1)\pi^{\frac{D-3}{2}} r_+^{3-D}\left(\frac{(D-3)q_e^2\left(\frac{1}{8\beta q_m^2 r_+^{4-2D}\Gamma(D-1)^2+1} - {}_2F_1\left(1, \frac{D-3}{2(D-2)}; \frac{7-3D}{4-2D}; -8\beta q_m^2 r_+^{4-2D}\Gamma(D-1)^2\right)\right)}{D-2} + 2q_m^2\right)}{32(D-3)q_m\Gamma\left(\frac{D+1}{2}\right)}. \tag{3.11}$$

To construct the black hole entropy, one use the Eq. (3.9) at constant parameters, which yields to

$$S = \int \frac{1}{T_+} dM = \int \frac{1}{T_+}\frac{dM}{dr_+} dr_+. \tag{3.12}$$

Inserting Eqs. (3.1)–(3.3) into (3.12), the entropy takes the following form

$$S = \frac{\omega}{4} r_+^{D-2}\left(1 + \frac{2\tilde{\alpha}}{r_+^2}\frac{D-2}{D-4}\right). \tag{3.13}$$

It is commonly known that the black hole stability is analyzed via the heat capacity sign; the black hole is stable when C_h is positive, or unstable if C_h is negative. The expression of this physical quantity is given by

$$C_h = \frac{\partial M}{\partial T_+} = \left(\frac{\partial M}{\partial r_+}\right)\left(\frac{\partial r_+}{\partial T_+}\right). \tag{3.14}$$

By using Eqs. (3.1) and (3.3) we get

$$C_h = \frac{c_1}{c_2}, \tag{3.15}$$

with

$$\begin{aligned} c_1 = &-(D-2)\,\omega\, r_+^D\left(2\tilde{\alpha} + r_+^2\right)^2\left(8\beta r_+^4\Gamma(D-1)^2 q_m^2 + r_+^{2D}\right) \\ &\times\left(\left(-2r_+^{2D}\left(2\Lambda r_+^4 - (D-3)(D-2)\left(\tilde{\alpha}\frac{D-5}{D-3} + r_+^2\right)\right)\right.\right. \\ &\left.\left.-r_+^8 q_m^2\right)\left(8\beta r_+^4\Gamma(D-1)^2 q_m^2 + r_+^{2D}\right) - r_+^{2D+8} q_e^2\right), \end{aligned} \tag{3.16}$$

$$\begin{aligned} c_2 = 4r_+^4\Bigg(&r_+^{2D+8} q_e^2\Big(8\beta r_+^4\Gamma(D-1)^2 q_m^2\left(6\tilde{\alpha} + r_+^2\right) \\ &+ r_+^{2D}\left((5-2D)r^2 - 2\tilde{\alpha}(2D-7)\right)\Big) \\ &+ \Bigg(r_+^8 q_m^2\left((5-2D)r_+^2 - 2\tilde{\alpha}(2D-7)\right) \\ &+ 2r_+^{2D}\Bigg((D-3)(D-2)\left(2\tilde{\alpha}^2\frac{D-5}{D-3} + \tilde{\alpha}\frac{D-9}{D-3}r_+^2 + r_+^4\right) \\ &+ 2\Lambda r_+^4\left(6\tilde{\alpha} + r_+^2\right)\Bigg)\Bigg)\left(8\beta r_+^4\Gamma(D-1)^2 q_m^2 + r_+^{2D}\right)^2\Bigg). \end{aligned} \tag{3.17}$$

It is clear that in the case of $\alpha = q_m = q_e = \Lambda = \beta = 0$ the heat capacity (3.15) reduces to

$$C_h = -\frac{1}{4}(D-2)r_+^{D-2}\omega, \tag{3.18}$$

which is the same result as [57].

The heat capacity behavior against r_+ is depicted in Fig. 3 showing the effect of the parameters D, α, Λ and q_m. One observes that the heat capacity C_+ is positive for $r_+ < r_c$ which means that the black hole is locally stable, whereas the heat capacity is negative for $r_c < r_+$, hence the black hole is locally unstable. Moreover, the heat capacity sign changes at $r_+ = r_c$ indicating that the second-order phase transition occurs there. With regards to Fig. 3a, it is remarkable that the r_c is sensitive to the variation of the dimension D. One can see that the r_c increases as the dimension D increases. Likewise, a similar effect is observed from the variation of the GB coupling constant on the changes of r_c, Fig. 4a. Whereas the critical radius r_c varies in full agreement with the variation of the cosmological constant Λ in such a way that r_c is shifted towards the right when the Λ value is increasing (cf. Fig. 3c). In addition to the prior cases, two divergent points r_{c1} and r_{c2} arise regarding the magnetic charge variation, generating three zones (cf. Fig. 3d). Indeed, at small horizon radii, the heat capacity is positive, yielding a stable small black hole. In what follows, the heat capacity becomes negative after crossing the first zone, involving an unstable intermediate black hole. The heat capacity rapidly changes its sign to be positive again, which means that the large black hole is locally stable. It is worth noting that for a certain fixed value of the magnetic charge, the divergent behavior of the heat capacity is completely eliminated. Furthermore, the critical radii r_{c1} and r_{c2} have the opposite behavior when we vary the magnetic charge. Specifically, at a small horizon radius r_+, r_{c1} is fully proportional to the q_m variation. In contrast, once q_m increases, the r_{c2} decreases at a large horizon radius. Similarly, the same behavior as in Fig. 3d is shown in Fig. 4 for the electric charge effect.

4 Black hole shadow

In this section,we will study the null geodesics, where the space-time geometry is described by (2.32). We use the Lagrangian and Hamilton–Jacobi equation to obtain the motion equations of the test particle.

We start with Lagrangian, given by

$$\mathcal{L} = \frac{1}{2}g_{\mu\nu}\dot{x}^\mu\dot{x}^\nu, \tag{4.1}$$

where $g_{\mu\nu}$ is the metric tensor, the dot denotes the derivative with respect to an affine parameter λ.

The canonically conjugate momentums solution provides,

$$P_t = \frac{E}{f(r)}, \tag{4.2}$$

$$P_r = \frac{1}{f(r)}\dot{r}, \tag{4.3}$$

$$P_{\theta_i} = r^2\sum_{i=1}^{D-3}\prod_{j=1}^{i-1}\sin^2\theta_j\,\dot{\theta}_i, \tag{4.4}$$

$$P_\phi = r^2\prod_{i=1}^{D-3}\sin^2\theta_i = L, \tag{4.5}$$

where E and L are the test particle's energy and angular momentum, respectively. In order to study the photon orbits around the black hole, the geodesics of such a particle must be derived. To achieve such a goal, we employ the Hamilton–Jacobi approach based on the Carter constant separable method in higher dimensions, which is given by

$$\frac{\partial S}{\partial\lambda} + \frac{1}{2}g^{\mu\nu}\frac{\partial S}{\partial x^\mu}\frac{\partial S}{\partial x^\nu} = 0, \tag{4.6}$$

where S is the Jacobi action. To solve the above equation, we assume the following anzats [32]

$$S = \frac{1}{2}m\lambda^2 - Et + L\phi + S_r(r) + \sum_{i=1}^{D-3}S_{\theta_i}(\theta_i), \tag{4.7}$$

where $S_r(r)$, $S_{\theta_i}(\theta_i)$ are functions of r and θ_i respectively, and m is the mass of the test particle, which equals zero as the photon. The substitution of Eq. (4.7) in Eq. (4.6) gives

$$\begin{aligned}-2\frac{\partial S}{\partial\lambda} = &-\frac{1}{f(r)}\left(\frac{\partial S_t}{\partial t}\right)^2 + f(r)\left(\frac{\partial S_r}{\partial r}\right)^2\\ &+\frac{1}{r^2\prod_{i=1}^{D-3}\sin^2\theta_i}\left(\frac{\partial S_\phi}{\partial\phi}\right)^2\\ &+\sum_{i=1}^{D-3}\frac{1}{r^2\prod_{j=1}^{i-1}\sin^2\theta_j}\left(\frac{\partial S_{\theta_i}}{\partial\theta_i.}\right)^2.\end{aligned} \tag{4.8}$$

By employing the separability method and introducing the Carter constant $\mathcal{K}$, we get

$$\begin{aligned}0 = &-\frac{1}{f(r)}\left(\frac{\partial S_t}{\partial t}\right)^2 + f(r)\left(\frac{\partial S_r}{\partial r}\right)^2\\ &+\frac{1}{r^2}\left(\frac{1}{\prod_{i=1}^{D-3}\sin^2\theta_i}\left(\frac{\partial S_\phi}{\partial\phi}\right)^2 + \mathcal{K} - \left(\frac{\partial S_\phi}{\partial\phi}\right)^2\prod_{i=1}^{D-3}\cot^2\theta_i\right)\\ &+\frac{1}{r^2}\left(\sum_{i=1}^{D-3}\frac{1}{\prod_{j=1}^{i-1}\sin^2\theta_j}\left(\frac{\partial S_{\theta_i}}{\partial\theta_i}\right)^2\right.\\ &\left.-\mathcal{K} + \left(\frac{\partial S_\phi}{\partial\phi}\right)^2\prod_{i=1}^{D-3}\cot^2\theta_i\right),\end{aligned} \tag{4.9}$$

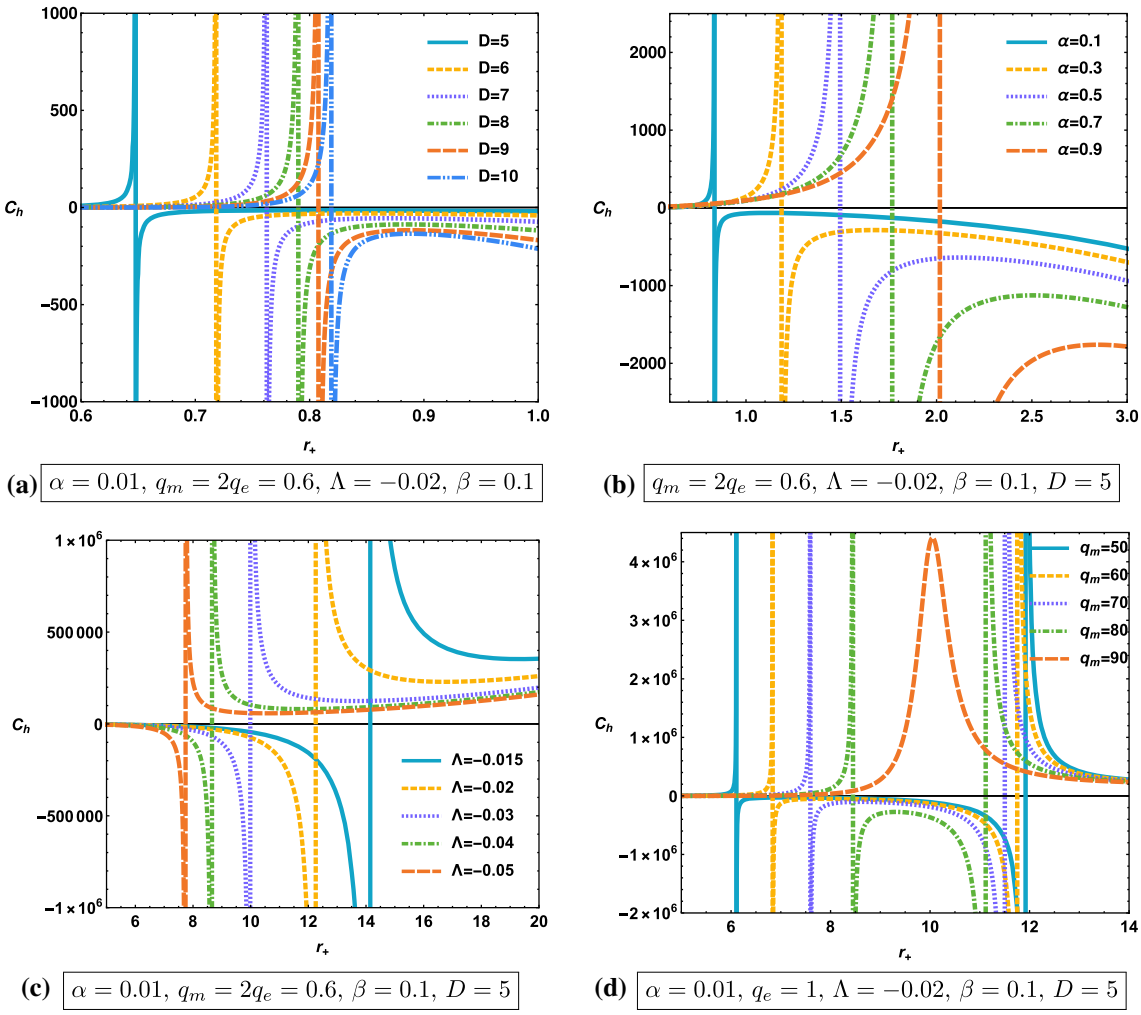

(a) $\alpha = 0.01,\ q_m = 2q_e = 0.6,\ \Lambda = -0.02,\ \beta = 0.1$ **(b)** $q_m = 2q_e = 0.6,\ \Lambda = -0.02,\ \beta = 0.1,\ D = 5$

(c) $\alpha = 0.01,\ q_m = 2q_e = 0.6,\ \beta = 0.1,\ D = 5$ **(d)** $\alpha = 0.01,\ q_e = 1,\ \Lambda = -0.02,\ \beta = 0.1,\ D = 5$

Fig. 3 The heat capacity behavior vs r_+ for various dimension (**a**), different GB coupling constant value (**b**), different values of Λ (**c**) and different values of q_m (**d**)

which can be written as follows:

$$0 = -\frac{E^2}{f(r)} + f(r)\left(\frac{\partial S_r}{\partial r}\right)^2 + \frac{1}{r^2}\left(\frac{L^2}{\prod_{i=1}^{D-3}\sin^2\theta_i} + \mathcal{K} - \prod_{i=1}^{D-3} L^2\cot^2\theta_i\right) + \frac{1}{r^2}\left(\sum_{i=1}^{D-3}\frac{1}{\prod_{j=1}^{i-1}\sin^2\theta_j}\left(\frac{\partial S_{\theta_i}}{\partial\theta_i}\right)^2 - \mathcal{K} + \prod_{i=1}^{D-3} L^2\cot^2\theta_i\right), \tag{4.10}$$

where we have used $\frac{\partial S_t}{\partial t} = E$, $\frac{\partial S_\phi}{\partial \phi} = L$,

By incorporating Eqs. (4.2)–(4.5) into Eq. (4.10), we can obtain the entire system of equations that govern the photon motion around the black hole, as follows:

$$\dot{t} = \frac{E}{f(r)}, \tag{4.11}$$

$$\dot{\phi} = \frac{L}{r^2\prod_{i=1}^{D-3}\sin^2\theta_i}, \tag{4.12}$$

$$r^2\dot{r} = \pm\sqrt{\mathcal{R}(r)}, \tag{4.13}$$

$$r^2\sum_{i=1}^{D-3}\prod_{j=1}^{i-1}\sin^2\theta_i\dot{\theta}_i = \pm\sqrt{\Theta_i(\theta_i)} \tag{4.14}$$

where

$$\mathcal{R}(r) = E^2r^4 - r^2 f(r)\left(\mathcal{K} + L^2\right), \tag{4.15}$$

$$\Theta_i(\theta_i) = \mathcal{K} - \prod_{i=1}^{D-3} L^2\cot^2\theta_i. \tag{4.16}$$

To obtain the boundary of the black hole shadow, one should study the radial equation. Thus, Eq. (4.13) can be reformulated as

$$\dot{r}^2 + V_{eff} = 0 \tag{4.17}$$

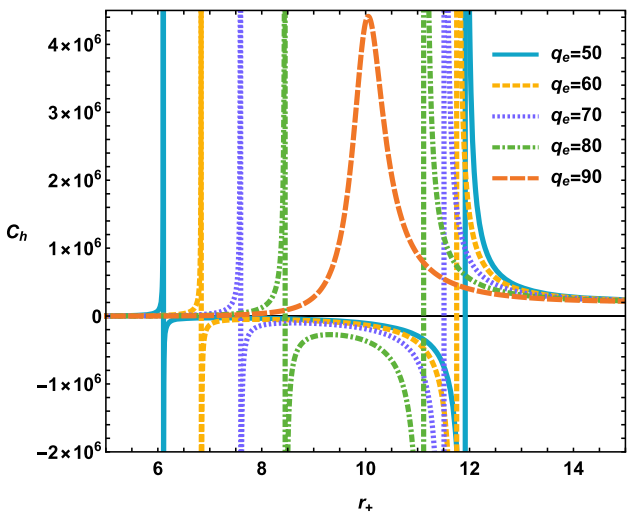

(a)

Fig. 4 The heat capacity behavior vs r_+ for different values of the electric charge, q_e, with $\alpha = 0.01$, $q_m = 1$, $\Lambda = -0.02$, $\beta = 0.1$ and $D = 5$

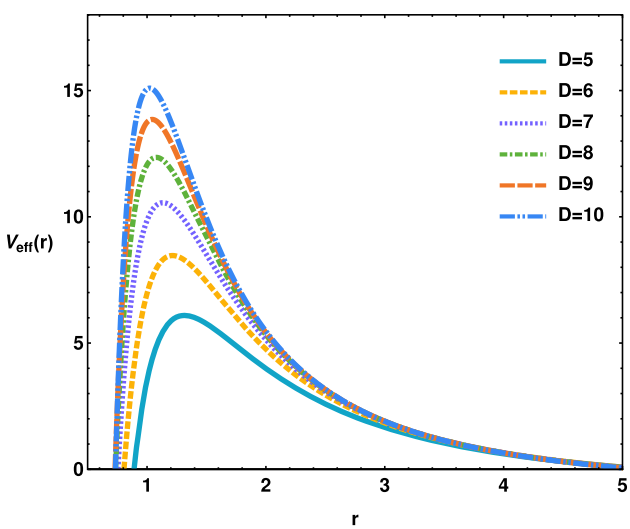

Fig. 5 The effective potential vs the radius coordinate behavior in various dimension for $m = 1$, $\mathcal{K} = 1$, $E = 1$ and $L = 5$

where $V_{eff}(r)$ is the effective potential for radial motion given by

$$V_{eff}(r) = \frac{f(r)}{r^2}\left(\mathcal{K} + L^2\right) - E^2. \tag{4.18}$$

In Fig. 5, we depict the effective potential as a function of the coordinate r to analyze its behavior as well as to look the effect of the dimension. From such figure, we can see that the potential has a maximum, which corresponds to an unstable orbit, and its value grows with increasing dimension. Furthermore, as we go $r \to \infty$, effective potential asymptotes to a constant value.

To find the unstable circular orbits that limit the apparent shape of the shadow of a black hole, we maximize the effective potential by setting the following conditions:

$$V_{eff}(r)\Big|_{r=r_p} = \frac{\partial V_{eff}(r)}{\partial r}\Big|_{r=r_p} = 0, \quad \text{or}$$
$$\mathcal{R}(r)\Big|_{r=r_p} = \frac{\partial \mathcal{R}(r)}{\partial r}\Big|_{r=r_p} = 0, \tag{4.19}$$

where r_p is the photon sphere radius. The radius of the photon sphere is given by the solution of the equation $V(r_p) = 0$. The acquired r_p is then entered into the equation $V'(r_p) = 0$ to see if the constraint $V''(r_p) < 0$ is satisfied in order to obtain the unstable photon orbits [58].

Now, using the condition $V_{eff}(r) = 0\Big|_{r=r_p}$ yields to

$$\frac{r_p^2}{f(r_p)} = \frac{L^2}{E^2} + \frac{\mathcal{K}}{E} = \xi^2 + \eta, \tag{4.20}$$

where we have adopted the definition of the impact parameters introduced in [59]

$$\frac{L}{E} = \xi, \quad \frac{\mathcal{K}}{E^2} = \eta. \tag{4.21}$$

In fact, we use the boundary constraint $\frac{\partial V_{eff}(r)}{\partial r}\Big|_{r=r_p} = 0$, to make the radius r_p of the photon sphere accurate. To reach that, we should resolve the following equation

$$rf'(r)\big|_{r=r_p} - 2f(r)\big|_{r=r_p} = 0. \tag{4.22}$$

However, in our case the above equation can not be solved analytically. So we solve it using a numerical method. The Table 1 outlines the findings

We now aim to determine the visible shape of the black hole shadow. For a better visualization, we use celestial coordinates X and Y_i to determine the location of the shadow. The coordinate X corresponds to the shape's apparent perpendicular distance as seen from the axis of symmetry, and the coordinate Y_i corresponds to the shape's apparent perpendicular distance as seen from its projection on the equatorial plane.

The celestial coordinates X and Y can be used to illustrate the apparent shape of the black hole shadow for an observer who is far away from the black hole. In accordance with [59] we can write

$$X = \lim_{r_0\to\infty}\left(\frac{r_0 P^{(\phi)}}{P^{(t)}}\right),$$
$$Y_i = \lim_{r_0\to\infty}\left(\frac{r_0 P^{(\theta_i)}}{P^{(t)}}\right), \quad i = 1, \ldots, D-3 \tag{4.23}$$

where r_0 is the distance from the black hole to the far observer. Furthermore, we calculate the above limits by using the canonically conjugate momentum Eqs. (4.2)–(4.5), and the

Table 1 The event horizon radius and photon sphere radius for variations in dimension D and the GB parameter α with $q_m = 2q_e$, $\Lambda = -0.02$, $\beta = 0.1$

$D(\alpha = 0.1)$	5	6	7	8	9	10
r_p	1.31476	1.2141	1.3332	1.07786	1.04324	1.02226
r_e	0.86855	0.790518	0.743893	0.726719	0.724342	0.728466
$\alpha(D = 5)$	0.1	0.15	0.185	0.2	0.25	0.3
r_p	1.31476	1.26797	1.23157	1.21484	1.15282	1.07707
r_e	0.86855	0.805181	0.756611	0.734407	0.65166	0.541573

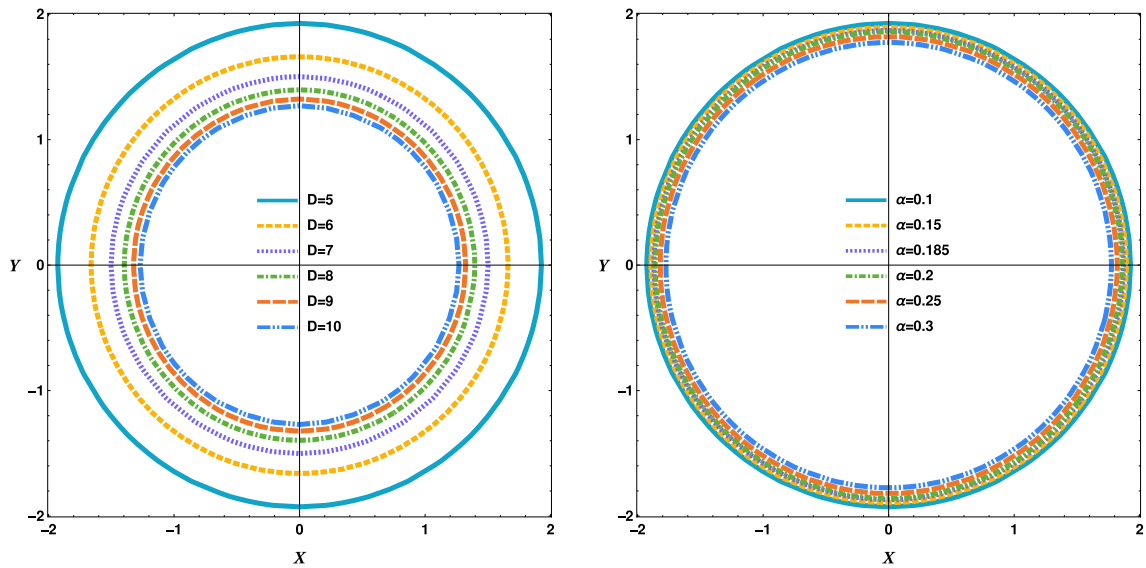

(a) $\alpha = 0.1,\ q_m = 2q_e = 0.6,\ \Lambda = -0.02,\ \beta = 0.1$ **(b)** $D = 5,\ q_m = 2q_e = 0.6,\ \Lambda = -0.02,\ \beta = 0.1$

Fig. 6 Black hole shadow in celestial plane $(X - Y)$ in different dimension D (left panel), and Gauss–Bonnet parameter α (right panel)

geodesic equation of motion (4.11)–(4.14), we obtains

$$X = \frac{-\xi \prod_{i=1}^{D-3} \csc\theta_i}{\sqrt{1 - \frac{(\eta+\xi^2)(1-\sqrt{1-\frac{8\tilde{\alpha}\Lambda}{(D-1)(D-2)}})}{2\tilde{\alpha}}}}, \tag{4.24}$$

$$Y_i = \pm\sqrt{\frac{\eta - \xi^2 \prod_{i=1}^{D-3} \cot^2\theta_i}{\sqrt{1 - \frac{(\eta+\xi^2)(1-\sqrt{1-\frac{8\tilde{\alpha}\Lambda}{(D-1)(D-2)}})}{2\tilde{\alpha}}}}}. \tag{4.25}$$

We will consider an observer on the equatorial hyperplane ($\theta_i = \frac{\pi}{2}$) for the sake of simplicity. The celestial coordinates can be written as

$$X = \frac{-\xi}{\sqrt{1 - \frac{(\eta+\xi^2)(1-\sqrt{1-\frac{8\tilde{\alpha}\Lambda}{(D-1)(D-2)}})}{2\tilde{\alpha}}}}, \tag{4.26}$$

$$Y = \pm\sqrt{\frac{\eta}{\sqrt{1 - \frac{(\eta+\xi^2)(1-\sqrt{1-\frac{8\tilde{\alpha}\Lambda}{(D-1)(D-2)}})}{2\tilde{\alpha}}}}}. \tag{4.27}$$

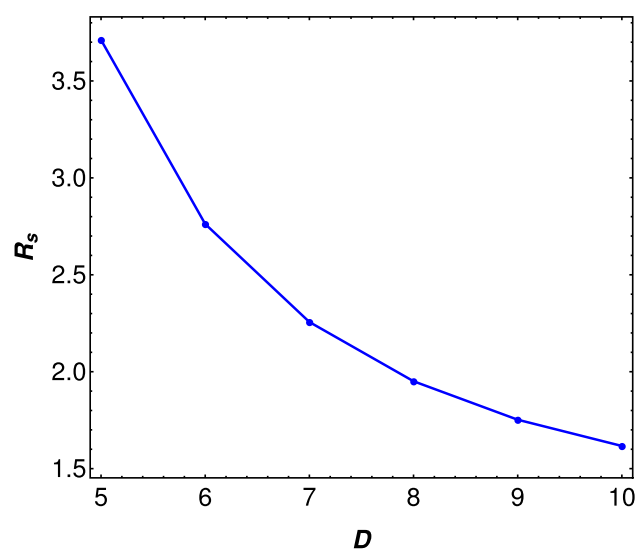

Fig. 7 The radius shadow behavior with respect to the dimension D for $m = 1$

Combining the coordinates X and Y yields an equation describing a circle with a radius of R_s in the celestial plane

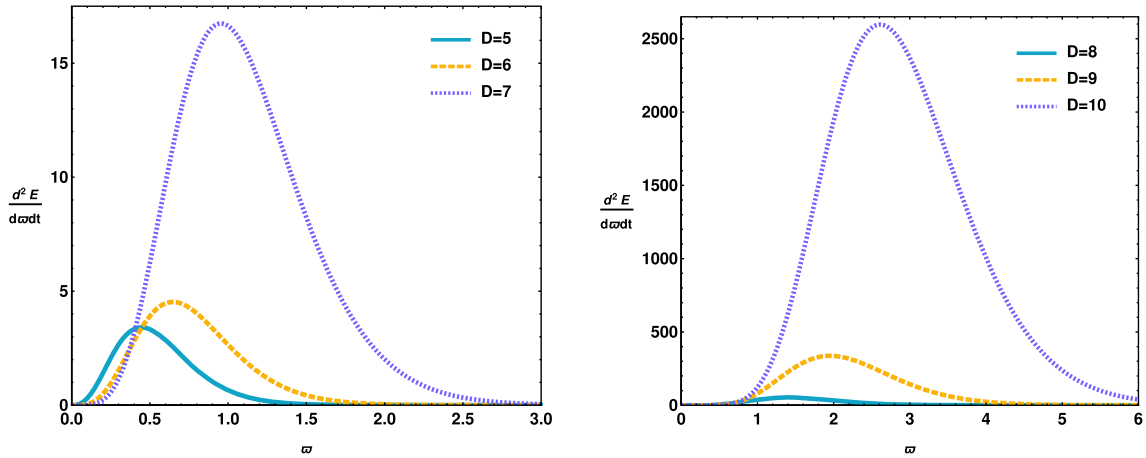

(a) $\alpha = 0.1,\ q_m = 2q_e = 0.6,\ \Lambda = -0.02,\ \beta = 0.1$ **(b)** $\alpha = 0.1,\ q_m = 2q_e = 0.6,\ \Lambda = -0.02,\ \beta = 0.1$

Fig. 8 The energy emission rate variation vs frequency ϖ for different dimension D for $m = 1$

$X - Y$, which is given by

$$R_s^2 = X^2 + Y^2 = \frac{\xi^2 + \eta}{1 - \frac{(\eta+\xi^2)(1-\sqrt{1-\frac{8\tilde{\alpha}\Lambda}{(D-1)(D-2)}})}{2\tilde{\alpha}}}. \tag{4.28}$$

By using Eq. (4.20), the radius shadow R_s becomes

$$R_s^2 = \frac{\frac{r_p^2}{f(r_p)}}{1 - \frac{r_p^2}{f(r_p)}\left(\frac{1-\sqrt{1-\frac{8\tilde{\alpha}\Lambda}{(D-1)(D-2)}}}{2\tilde{\alpha}}\right)}, \tag{4.29}$$

which results in

$$R_s = \sqrt{\frac{\frac{r_p^2}{f(r_p)}}{1 - \frac{r_p^2}{f(r_p)}\left(\frac{1-\sqrt{1-\frac{8\tilde{\alpha}\Lambda}{(D-1)(D-2)}}}{2\tilde{\alpha}}\right)}}. \tag{4.30}$$

As shown in Fig. 6, we plot black hole shadows for various cases. The size of the black hole's shadow can be seen to be controlled by the dimension of space-time D and the Gauss–Bonnet parameter α. According to Fig. 6a the black hole shadow has a circular shape, and the size of this circle increases as D increases. Furthermore, the same behavior has been noticed with the increase of α in Fig. 6b (Fig. 7).

5 Energy emission rates

In this section, we study the energy emission rate (EER) in the D-dimension. Several studies have demonstrated the analysis of the energy emission rate with respect to the parameter dimension D as well as the coupling constant of the Gauss–Bonnet gravity α [60,61]. For a faraway observer, it is well known that the shadow is responsible for a high energy absorption cross section due to the black hole. The energy emission rate of a black hole in a higher dimension can be expressed as [62],

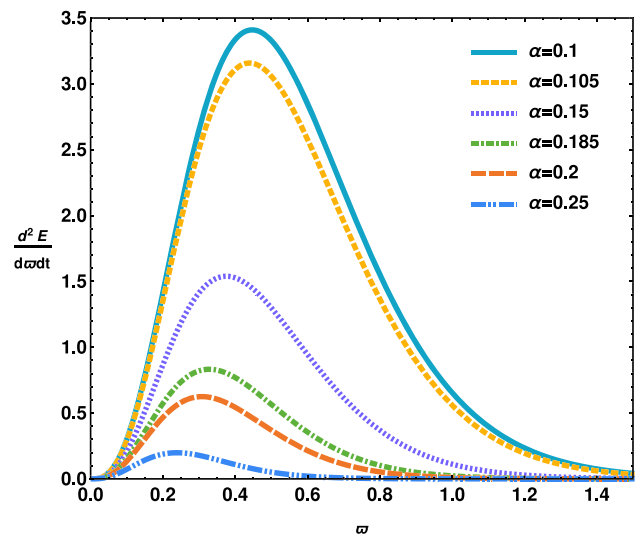

(a) $D = 5,\ q_m = 2q_e = 0.6,\ \Lambda = -0.02,\ \beta = 0.1$

Fig. 9 The energy emission rate variation vs frequency ϖ for different GB constant α for $m = 1$

$$\frac{d^2E(\varpi)}{d\varpi dt} = \frac{2\pi^2\sigma_{lim}}{\exp\left(\frac{\varpi}{T_H}\right) - 1}\varpi^{(D-1)} \tag{5.1}$$

where ϖ is the frequency, T_H is the Hawking temperature given by (3.4), and σ_{lim} is the limiting constant value for an absorption cross section oscillating around a spherically symmetric black hole.

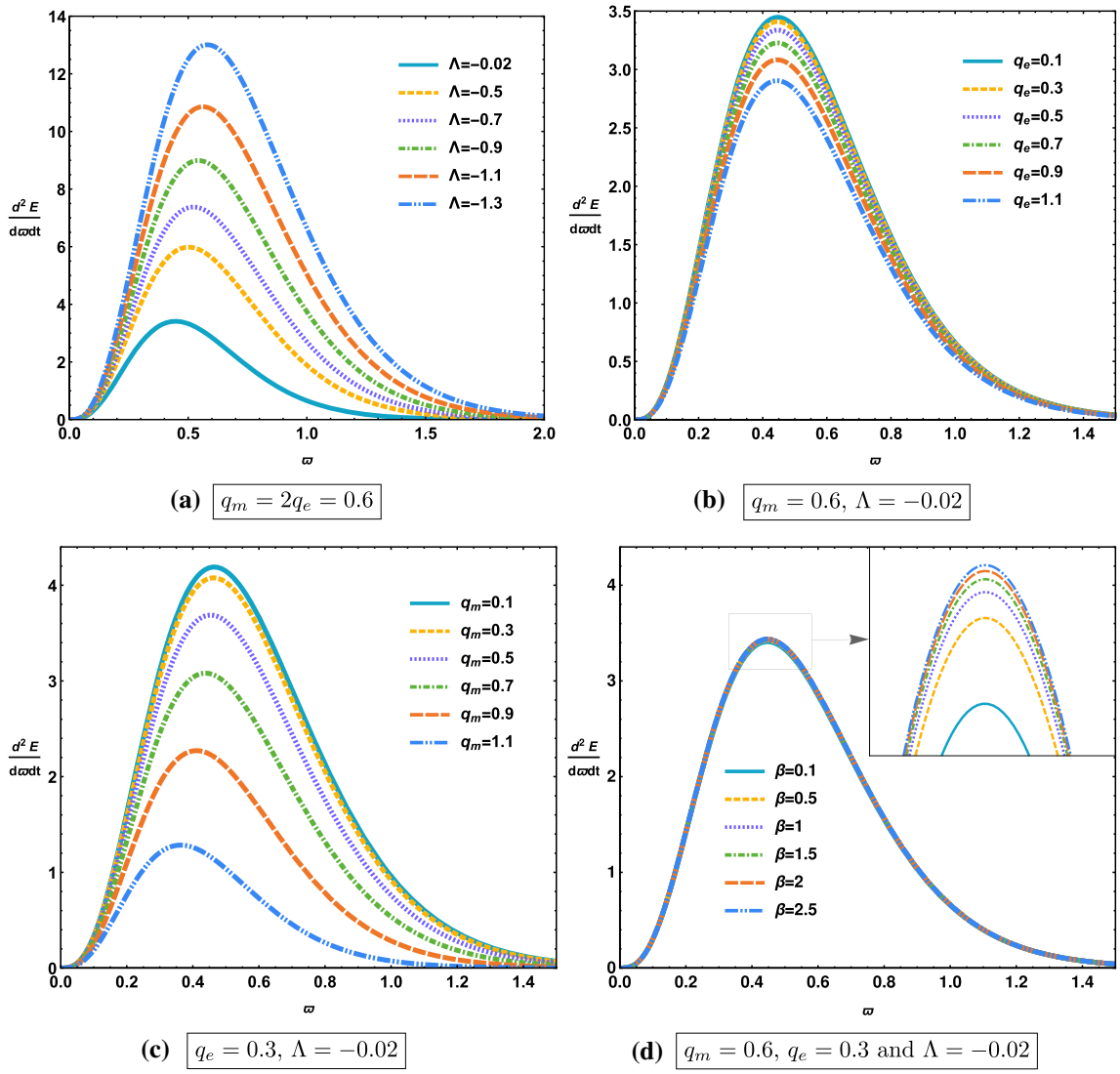

(a) $q_m = 2q_e = 0.6$ **(b)** $q_m = 0.6,\ \Lambda = -0.02$

(c) $q_e = 0.3,\ \Lambda = -0.02$ **(d)** $q_m = 0.6,\ q_e = 0.3$ and $\Lambda = -0.02$

Fig. 10 The energy emission rate variation vs frequency ϖ for Λ (**a**), q_e (**b**) and q_m (**c**) with $m = 1$, $D = 5$ and $\beta = 0.1$

A D-dimensional black hole's limiting constant value σ_{lim} can be approximated by [63]

$$\sigma_{lim} = \frac{\pi^{(\frac{D-2}{2})} R_s^{(D-2)}}{\Gamma(\frac{D}{2})} \tag{5.2}$$

where R_s is the radius shadow.

Figure 8 shows the energy emission rate against the frequency ϖ in various dimensions D. We can see that there is a peak in the energy emission rate for the black hole. Concretely, this peak becomes greater with an increase in dimension D. Therefore, the evaporation process will be faster in higher-dimensional space-time, Fig. 8a, b. Furthermore, a similar explanation may be given for the effect of the Gauss–Bonnet constant α, Fig. 9.

Figure 10 indicates the variation of the energy emission rate as a function of the frequency ϖ for different values of Λ, q_e, and q_m. Generally, it is shown that the EER increases until such a peak, then it drops down to vanish. The peak of the EER appears to increase with decreasing Λ, as shown in Fig. 10a. While both the electric and magnetic charges have a similar effect on peak variation, Fig. 10b, c shows that as the latter parameters increase, the EER peak decreases. Furthermore, It is known that the coupling constant β gives rise to dual fields and hence to dyonic objects. The Fig. 10d shows the variation of the EER with respect to different fixed values of the coupling constant β. It is shown that, contrary to the previous Fig. 10a–c, increasing the coupling constant β causes the same variation in the EER peak. In other words, when the electric and magnetic interaction is strong, the evaporation process becomes faster for the dyonic AdS black hole system.

6 Conclusion

In this paper, we have derived a solution for a dyonic quasitopological electromagnetic source in the EGB gravity framework. The obtained solution brings us back to our usual solutions across the cancellation of some parameter space.

We have examined the thermodynamic aspects of the obtained solution, including the relevant ADM mass, Hawking temperature, and entropy. These last quantities have been employed to compute the heat capacity, which gives us the possibility to analyze the local stability. It was discovered that there are two distinct phases, each of which is located near the critical radius r_c. In the left region of r_c, we have a stable phase, whereas in the right region, we have an unstable phase state. The second phase transition has occurred at the critical radius of r_c. The critical radius, r_c, is proportionally affected by the parameters D and α. Moreover, it has been shown that the variation of r_c is compatible with the negative cosmological constant. In addition, the variations of the electric and magnetic charges have a similar effect on the heat capacity behavior.

Concerning the optical properties of this black hole, the behavior of its shadow has been studied. In brief, the Hamilton–Jacobi method was employed to integrate the geodesic equation of the test particle using Carter's separation of variables trick. We found that the shadow of this black hole has a circular shape whose radius depends on the value of the different parameters. We limited our study just to the effect of the parameter D and the GB coupling constant. We discovered that the increase in the parameter D and the GB coupling constant reduced the size of the shadow. The energy emission rate was discovered to vary in contrast to the parameters D, GB coupling constant α, the cosmological constant Λ, the electric q_e and the magnetic charge q_m.

This work comes up with open questions mainly related to the recent $4D$ EGB gravity as well as the phase transition study, which will be the next interesting topic.

Acknowledgements The authors would like to thank the anonymous referee for interesting comments and suggestions.

Data Availability Statement This manuscript has no associated data or the data will not be deposited. [Authors' comment: This work has no associated data.]

Funded by SCOAP^3. SCOAP^3 supports the goals of the International Year of Basic Sciences for Sustainable Development.

References

1. H.-S. Liu, Z.-F. Mai, Y.-Z. Li, H. Lu, Quasi-topological electromagnetism: dark energy, dyonic black holes, stable photon spheres and hidden electromagnetic duality. Sci. China Phys. Mech. Astron. **63**, 240411 (2020). arXiv:1907.10876 [hep-th]
2. J.D. Bekenstein, Black holes and the second law. Lett. Nuovo Cim. **4**, 737–740 (1972)
3. J.D. Bekenstein, Black holes and entropy. Phys. Rev. D **7**, 2333–2346 (1973)
4. J.M. Bardeen, B. Carter, S.W. Hawking, The four laws of black hole mechanics. Commun. Math. Phys. **31**, 161–170 (1973)
5. S.W. Hawking, Particle creation by black holes. Commun. Math. Phys. **43**, 199–220 (1975)
6. D. Kastor, S. Ray, J. Traschen, Enthalpy and the mechanics of AdS black holes. Class. Quantum Gravity **26**, 195011 (2009). arXiv:0904.2765
7. D. Kubiznak, R.B. Mann, M. Teo, Black hole chemistry: thermodynamics with Lambda. Class. Quantum Gravity **34**, 063001 (2017). arXiv:1608.06147
8. D. Kubiznak, R.B. Mann, P–V criticality of charged AdS black holes. JHEP **1207**, 033 (2012). arXiv:1205.0559
9. C.V. Johnson, Holographic heat engines. Class. Quantum Gravity **31**, 205002 (2014). arXiv:1404.5982
10. H. Xu, Y. Sun, L. Zhao, Black hole thermodynamics and heat engines in conformal gravity. Int. J. Mod. Phys. D **26**(13), 1750151 (2017). arXiv:1706.06442
11. M. Maldacena, The large N limit of superconformal field theories and supergravity. Adv. Theor. Math. Phys. **2**, 231–252 (1998)
12. G. 't Hooft, Dimensional reduction in quantum gravity. Conf. Proc. C **930308**, 284–296 (1995)
13. L. Susskind, The world as a hologram. J. Math. Phys. **36**, 6377–6396 (1995). arXiv:hep-th/9409089
14. C. Lanczos, Z. Phys. **73**, 147 (1932)
15. C. Lanczos, Ann. Math. **39**, 842 (1938)
16. D. Lovelock, J. Math. Phys. **12**, 498 (1971)
17. S.A. Pavluchenko, General features of Bianchi-I cosmological models in Lovelock gravity. Phys. Rev. D **80**, 107501 (2009). arXiv:0906.0141 [gr-qc]
18. P. Wang, H. Wu, H. Yang, S. Ying, Derive Lovelock gravity from string theory in cosmological background. JHEP **05**, 218 (2021). arXiv:2012.13312 [hep-th]
19. C. Callan, I. Klebanov, M. Perry, String theory effective actions. Nucl. Phys. B **278**, 78 (1986)
20. P. Candelas, G. Horowitz, A. Strominger, E. Witten, Vacuum configurations for superstrings. Nucl. Phys. B **258**, 46 (1985)
21. D. Gross, J. Sloan, The quartic effective action for the heterotic string. Nucl. Phys. B **291**, 41 (1987)
22. M. Guica, L. Huang, W. Li, A. Strominger, R2 corrections for 5D black holes and rings. J. High Energy Phys. **0610**, 036 (2006)
23. K. Kashima, The M2-brane solution of heterotic M-theory with the Gauss–Bonnet R2 terms. Prog. Theor. Phys. **105**, 301–321 (2001). arXiv:hep-th/0010286
24. D.G. Boulware, S. Deser, Phys. Rev. Lett. **55**, 2656 (1985)
25. J.T. Wheeler, Nucl. Phys. B **268**, 737 (1986)
26. R.C. Myers, J.Z. Simon, Black-hole thermodynamics in Lovelock gravity. Phys. Rev. D **38**, 2434 (1988)

27. A. Kumar, D. Veer Singh, S.G. Ghosh, *D*-dimensional Bardeen-AdS black holes in Einstein–Gauss–Bonnet theory. Eur. Phys. J. C **79**(3), 275 (2019). arXiv:1808.06498 [gr-qc]
28. D. Glavan, C. Lin, Einstein–Gauss–Bonnet gravity in 4-dimensional space-time. Phys. Rev. Lett. **124**(8), 081301 (2020). arXiv:1905.03601
29. B. Eslam Panah, Kh. Jafarzade, S.H. Hendi, Charged 4D Einstein–Gauss–Bonnet–AdS black holes: shadow, energy emission, deflection angle and heat engine. Nucl. Phys. B **961**, 115269 (2020)
30. P.G.S. Fernandes, Charged black holes in AdS spaces in 4D Einstein Gauss–Bonnet gravity. Phys. Lett. B **805**, 135468 (2020)
31. S.A. Hosseini Mansoori, Thermodynamic geometry of the novel 4-D Gauss–Bonnet AdS black hole. Phys. Dark Universe **31**, 100776 (2021). arXiv:2003.1338
32. B.P. Singh, S.G. Ghosh, Shadow of Schwarzschild–Tangherlini black holes. Ann. Phys. **395**, 127–137 (2018). arXiv:1707.07125 [gr-qc]
33. A. Strominger, Les Houches lectures on black holes. arxiv:hep-th/9501071
34. K. Akiyama et al. (Event Horizon Telescope), First M87 Event Horizon Telescope results. IV. Imaging the central supermassive black hole. Astrophys. J. Lett. **875**(1), L4 (2019). arXiv:1906.11241 [astro-ph.GA]
35. K. Akiyama et al. (Event Horizon Telescope), First M87 Event Horizon Telescope results. I. The shadow of the supermassive black hole. Astrophys. J. Lett. **875**, L1 (2019). arXiv:1906.11238 [astro-ph.GA]
36. A. Belhaj, Y. Sekhmani, Thermodynamics of Ayón-Beato–García–AdS black holes in 4D Einstein–Gauss–Bonnet gravity. Eur. Phys. J. Plus **137**(2), 278 (2022)
37. M. Guo, P.C. Li, Innermost stable circular orbit and shadow of the 4*D* Einstein–Gauss–Bonnet black hole. Eur. Phys. J. C **80**(6), 588 (2020). arXiv:2003.02523
38. R.A. Konoplya, A.F. Zinhailo, Quasinormal modes, stability and shadows of a black hole in the 4D Einstein–Gauss–Bonnet gravity. Eur. Phys. J. C **80**(11), 1049 (2020). arXiv:2003.01188
39. R. Kumar, S.G. Ghosh, Rotating black holes in 4*D* Einstein–Gauss–Bonnet gravity and its shadow. JCAP **07**, 053 (2020). https://doi.org/10.1088/1475-7516/2020/07/053. arXiv:2003.08927
40. A. Belhaj, Y. Sekhmani, Optical and thermodynamic behaviors of Ayón-Beato–García black holes for 4D Einstein Gauss–Bonnet gravity. Ann. Phys. **441**, 168863 (2022)
41. A. Das, A. Saha, S. Gangopadhyay, Shadow of charged black holes in Gauss–Bonnet gravity. Eur. Phys. J. C **80**(3), 180 (2020). arXiv:1909.01988 [gr-qc]
42. T. Hertog, T. Lemmens, B. Vercnocke, Imaging higher dimensional black objects. Phys. Rev. D **100**(4), 046011 (2019). arXiv:1903.05125 [hep-th]
43. A. Belhaj, Y. Sekhmani, Shadows of rotating quintessential black holes in Einstein–Gauss–Bonnet gravity with a cloud of strings. Gen. Relativ. Gravit. **54**(2), 17 (2022)
44. M. Born, L. Infeld, Foundations of the new field theory. Proc. R. Soc. Lond. A **144**(852), 425 (1934). https://doi.org/10.1098/rspa.1934.005
45. W. Heisenberg, H. Euler, Z. Phys. **98**, 714 (1936). arXiv:physics/0605038
46. I. Bandos, K. Lechner, D. Sorokin, P.K. Townsend, A non-linear duality-invariant conformal extension of Maxwell's equations. Phys. Rev. D **102**, 121703 (2020). arXiv:2007.09092 [hep-th]
47. J. Oliva, S. Ray, A new cubic theory of gravity in five dimensions: black hole, Birkhoff's theorem and C-function. Class. Quantum Gravity **27**, 225002 (2010). https://doi.org/10.1088/0264-9381/27/22/225002. arXiv:1003.4773 [gr-qc]
48. R.C. Myers, B. Robinson, Black holes in quasi-topological gravity. JHEP **1008**, 067 (2010). https://doi.org/10.1007/JHEP08(2010)067. arXiv:1003.5357 [gr-qc]
49. M.H. Dehghani, A. Bazrafshan, R.B. Mann, M.R. Mehdizadeh, M. Ghanaatian, M.H. Vahidinia, Black holes in quartic quasitopological gravity. Phys. Rev. D **85**, 104009 (2012). https://doi.org/10.1103/PhysRevD.85.104009. arXiv:1109.4708 [hep-th]
50. Y.Z. Li, H.S. Liu, H. Lü, Quasi-topological Ricci polynomial gravities. JHEP **1802**, 166 (2018). https://doi.org/10.1007/JHEP02(2018)166. arXiv:1708.07198 [hep-th]
51. A. Cisterna, G. Giribet, J. Oliva, K. Pallikaris, Quasitopological electromagnetism and black holes. Phys. Rev. D **101**(12), 124041 (2020). arXiv:2004.05474 [hep-th]
52. M.D. Li, H.M. Wang, S.W. Wei, Triple points and novel phase transitions of dyonic AdS black holes with quasi-topological electromagnetism. Phys. Rev D **105**(10), 104048. (2022). arXiv:2201.09026 [gr-qc]
53. S.G. Ghosh, U. Papnoi, S.D. Maharaj, Cloud of strings in third order Lovelock gravity. Phys. Rev. D **90**(4), 044068 (2014). arXiv:1408.4611 [gr-qc]
54. A. Ishibashi, H. Kodama, Stability of higher dimensional Schwarzschild black holes. Prog. Theor. Phys. **110**, 901 (2003). arXiv:hep-th/0305185
55. R.C. Myers, J.Z. Simon, Black hole thermodynamics in Lovelock gravity. Phys. Rev. D **38**, 2434–2444 (1988). https://doi.org/10.1103/PhysRevD.38.2434
56. S.G. Ghosh, D.W. Deshkar, Horizons of radiating black holes in Einstein Gauss–Bonnet gravity. Phys. Rev. D **77**, 047504 (2008). arXiv:0801.2710 [gr-qc]
57. S.G. Ghosh, U. Papnoi, S.D. Maharaj, Cloud of strings in third order Lovelock gravity. Phys. Rev. D **90**(4), 044068 (2014). arXiv:1408.4611 [gr-qc]
58. R. Roy, S. Chakrabarti, Study on black hole shadows in asymptotically de Sitter spacetimes. Phys. Rev. D **102**, 024059 (2020). arXiv:2003.14107 [gr-qc]
59. S. Chandrasekhar, *The Mathematical Theory of Black Holes* (Oxford University Press, Oxford, 1998)
60. P. Kanti, Black holes in theories with large extra dimensions: a review. Int. J. Mod. Phys. A **19**, 4899 (2004). arXiv:hep-ph/0402168
61. J. Grain, A. Barrau, P. Kanti, Exact results for evaporating black holes in curvature-squared lovelock gravity: Gauss–Bonnet greybody factors. Phys. Rev. D **72**, 104016 (2005)
62. S.W. Wei, Y.X. Liu, Observing the shadow of Einstein–Maxwell-Dilaton-Axion black hole. JCAP **11**, 063 (2013). arXiv:1311.4251 [gr-qc]
63. Y. Decanini, A. Folacci, B. Raffaelli, Fine structure of high-energy absorption cross sections for black holes. Class. Quantum Gravity **28**, 175021 (2011). arXiv:1104.3285 [gr-qc]